



ELSEVIER

Journal of Volcanology and Geothermal Research 73 (1996) 245–266

 Journal of volcanology
and geothermal research

Redistribution of Pb and other volatile trace metals during eruption, devitrification, and vapor-phase crystallization of the Bandelier Tuff, New Mexico

James Stimac^{a,*}, Donald Hickmott^a, Russell Abell^{a,1}, Adrienne C.L. Larocque^{a,2},
David Broxton^a, Jamie Gardner^a, Steve Chipera^a, John Wolff^b, Eric Gauerke^c

^a Earth and Environmental Sciences, EES-1, MS-D462, Los Alamos National Laboratory, Los Alamos, NM 87545, USA

^b Department of Geology, University of Texas at Arlington, Box 19049, Arlington, TX 76019, USA

^c Department of Geological Sciences, University of New Mexico, 200 Yale Blvd. NE, Albuquerque, NM 87131-1116, USA

Received 20 February 1995; accepted 11 February 1996

Abstract

A diverse suite of micron-scale minerals was deposited from vapor during eruption and post-emplacement crystallization of the Bandelier Tuff, New Mexico. The mineral suite is rich in sulfides, oxides, and chlorides of both common and rare metals (e.g., Fe, Pb, Bi, Cu, Ag, Re), and oxides and silicates of incompatible elements (e.g., P, Zr, Y, Nb, Ba and LREE). Minerals preserved in glassy samples grew from magmatic vapor trapped during emplacement, or from vapor migrating along contacts with more impermeable rocks; minerals observed in devitrified samples also grew from crystallization of glass and vapor liberated during this process. In devitrified samples, mafic silicate phenocrysts were partially replaced by an assemblage dominated by smectite and hematite.

The syn- to post-eruptive mineral assemblage observed in upper Bandelier Tuff (UBT) samples bears striking similarity to those deposited by cooling gases near active volcanic vents. However, several differences exist: (1) the mineral suite in the UBT is disseminated throughout the unit, and formed over a broad temperature range (> 700 to < 150°C) at higher rock:gas ratios; (2) the highly evolved composition of the UBT yielded a greater abundance of minerals rich in incompatible elements compared to sublimates from less evolved volcanoes; and (3) the UBT has suffered over 1 million years of post-emplacement exposure, which resulted in solution (or local re-precipitation in fractures) of soluble compounds such as halite, sylvite, and gypsum.

Pb was enriched toward the roof of the UBT magma body due to its affinity for the melt and vapor phases relative to crystals (Bulk $D_{Pb} < 0.2$). Micron-scale Pb minerals appear to have grown from vapor exsolved during eruption, as well as vapor liberated during later devitrification. Additional Pb was scavenged by smectite and hematite that probably formed during the later stages of the devitrification and cooling process. Up to ten-fold increases in Pb concentrations are seen in zones of fumarolic concentration in the UBT, however, most bulk tuff samples have Pb values that appear to preserve magmatic values, indicating only very local trace-metal redistribution. The concentration of Pb and other heavy metals in

* Corresponding author. Department of Geological Sciences, University of Manitoba, Winnipeg, Man. R3T 2N2, Canada

¹ Present address: I.C.F. Kaiser Engineers, Inc., 1900 Diamond Dr., Los Alamos, NM 87544, USA.

² Present address: Department of Geological Sciences, University of Manitoba, Winnipeg, Man. R3T 2N2, Canada.



micron-scale mineral coatings in porous tuff indicates that these metals could be readily mobilized and transported by acidic groundwaters or hydrothermal fluids, and thus locally concentrated into ore-grade deposits in long-lived systems.

Keywords: Pb; volatile; devitrification; Bandelier Tuff; metal mobility; metal partitioning; vapor transport

1. Introduction

Evidence from volcanic plumes and fumarolic sublimates indicates that certain elements are fractionated into the vapor phase during eruption and shallow degassing of magmas (Stoiber and Rose, 1974; Zoller et al., 1983; Symonds and Reed, 1993; Hinkley et al., 1994). Of particular interest are high concentrations of metals (As, Sb, Hg, Bi, Cd, Cu, In, Ag, Au, Re, Mo, Sn, W and Pb) in vapor associated with some intermediate-to-silicic systems (e.g., Symonds et al., 1987; Bernard et al., 1990; Kyle et al., 1990; Meeker et al., 1991; Papike et al., 1991; Webster and Duffield, 1991; Goff et al., 1994). Understanding the timing of release and natural fluxes of these elements in volcanic systems is important, both because of their potentially negative impact on human health and because of the significant economic importance of some of these metals. In this paper we assess the possible release and redistribution of volatile metals (particularly Pb) during the eruption process and during subsequent post-emplacment degassing, crystallization, and cooling of the Bandelier Tuff.

Aside from studies of fossil fumaroles (e.g., Keith, 1991; Papike et al., 1991) and of topaz- and tin-bearing rhyolites (Burt and Sheridan, 1981; Christiansen et al., 1986), few attempts have been made to document the trace-mineral assemblages formed during eruption and post-emplacment crystallization of volcanic rocks. In this study, we used scanning-electron microscopy (SEM), electron-microprobe (EMP) analysis and proton-induced X-ray emission (PIXE) analysis to characterize the trace-mineral assemblage in the Bandelier Tuff and to place some constraints on both the timing and extent of trace-element redistribution. The trace-mineral suite observed is similar to that composing fumarolic sublimates, but is present throughout the Bandelier Tuff on surfaces in both glassy tephra and devitrified tuff. We have quantified Pb abundances in phenocrysts, matrix glass and syn- to post-eruptive minerals, to evaluate the

significance of vapor/melt partitioning in silicic magmas and vapor-phase redistribution of metals in cooling ash sheets. We conclude that some fraction of volatile metals like Pb, present in the Bandelier magma at depth, was partitioned into the vapor phase during eruption, leading to crystallization of Pb minerals from trapped gases on glassy tephra. We also show that a portion of the Pb remaining in the melt (glass) was locally mobilized in gases evolved during devitrification and vapor-phase crystallization. This multi-stage redistribution of Pb (and other volatile metals) into micron-scale mineral coatings in porous tuff has broad implications for: (1) the importance of vapor/melt partitioning of volatile metals in magmatic systems; (2) petrogenetic interpretations of whole-rock volatile-element data (in both glassy and devitrified rocks); (3) characterization of background levels of toxic volatile metals in rocks and soils; (4) determining the source of metals in hydrothermal ore deposits associated with volcanic and shallow plutonic rocks; and (5) understanding and predicting trace-element mobility during *in situ* vitrification of contaminated rocks and soils.

2. Analytical methods

Many factors make positive identification of trace-mineral species difficult, including their: (1) small grain size (generally < 1–10 μm); (2) trace abundance (< 1 vol.%); (3) fragility; and (4) location in vesicles. The first two factors complicate both quantitative microanalysis and separation for X-ray diffraction studies, whereas the third and fourth factors reduce the likelihood that such grains will be observed in standard petrographic thin sections unless care is taken to preserve them. Finally, the inability of energy-dispersive spectrometry (EDS) analysis to detect light elements hampers positive identification of species such as oxides, hydroxides and carbonates. Our approach was to examine carefully prepared thin sections and freshly broken

pumice fragments with backscattered electrons to identify trace phases with high average atomic number. We then identified the major cations in selected minerals by a combination of EDS spectra and wavelength-dispersive spectrometry (WDS) scans, and where exceptionally large grains were present, analyzed them by WDS. X-ray diffraction studies were done when sufficient material could be separated for analysis.

When grain size permitted, we used electron-microprobe (EMP) and proton-induced X-ray emission (PIXE) analysis to characterize the major- and trace-element contents of minerals and glass. Wavelength-dispersive EMP data for minerals and glass were obtained on a Cameca SX50 electron microprobe operating at 15 keV accelerating potential with a 15 nA beam current, and corrected using the PAP scheme (Pouchou and Pichoir, 1985). Beam size was typically 5–10 μm for minerals, and 5–20 μm for glass (larger beam to mitigate Na loss), depending on whether bubble-wall textures permitted use of a larger spot. Major-element concentrations determined by EMP were used for standardization and reduction of PIXE data. PIXE analyses were obtained with the Los Alamos nuclear microprobe using methods described in Duffy et al. (1987), Burnett et al. (1988) and Stimac and Hickmott (1994). The low continuum background produced by proton beams allows for detection of many trace elements at concentrations of < 10 ppm. We operated the nuclear microprobe at an accelerating potential of 3 MeV, and beam currents of 10–20 nA. Samples were mounted on pure silica glass and analyzed with beam diameters from 5 to 20 μm for an average of 15 minutes. One-sigma counting statistic errors for individual PIXE analyses are given in parentheses in data tables, and the minimum detection limit is taken as 3 sigma. The accuracy and precision of PIXE analyses can be assessed by analysis of KH-1, a clinopyroxene reference standard from Kilborne Hole, NM. Repeated analysis of this standard over several years yielded mean trace-element concentrations that were within the range reported in a similar study by Czamanske et al. (1993), with standard deviations of ± 6 to 12% relative. Some mafic minerals were partially altered to micron-scale intergrowths of smectite and hematite. Additionally, some vapor-phase alkali feldspar was intergrown with silica

polymorphs at the scale of analysis. It was impossible to get "clean" PIXE analyses of these materials, therefore analyses thought to suffer from such contamination are listed as semi-quantitative, and are discussed further in the results section.

We characterized the major- and trace-element concentrations of bulk tuff samples by X-ray fluorescence (XRF) analysis using procedures described by Stimac et al. (1995). X-ray diffraction (XRD) analysis was used to quantify mineral compositions of bulk tuff samples, and identify alteration minerals associated with pyroxene phenocrysts. Data were collected on a Siemens D-500 diffractometer using Cu-K α radiation, incident- and diffracted-beam Soller slits and a Kevex solid-state (SiLi) detector. Quantitative XRD analyses of bulk tuff employed the internal-standard method of Chung (1974), which requires the addition of an internal standard (corundum) to each sample. Analytical details have been described by Bish and Chipera (1988) and Broxton et al. (1995). Sample preparation for qualitative XRD analyses of smectitic coatings on pyroxene grains involved suspending samples in acetone and depositing them onto an off-axis cut (zero background) quartz plate. In addition, samples were solvated overnight in an ethylene-glycol atmosphere to determine the amount of expansion and confirm the presence of smectite. Graphite-furnace atomic absorption (GFAA) analysis was used to determine the concentrations of a suite of metals including Pb in bulk tuff samples. Samples were digested in acid and analyzed with a Perkin Elmer HGA-500 furnace. Analyses of reference standards indicate accuracies of $\pm 5\%$ for Co, Cu and Pb and ± 30 –50% for Cr, Mo and Ni. Precisions determined by replicate analyses were $\pm 5\%$ or less for Cu, Mo, Pb and Zn, and ± 20 to 35% for Cr and Ni.

3. Geological background

The Bandelier Tuff is composed of the Otowi (Lower) and Tshirege (Upper) members, each consisting of a basal plinian fallout pumice bed with overlying ash-flow deposits. The Otowi Member was erupted 1.61 million years ago (Izett and Obradovich, 1994), during the first major episode of caldera formation. It is a single cooling unit with a volume

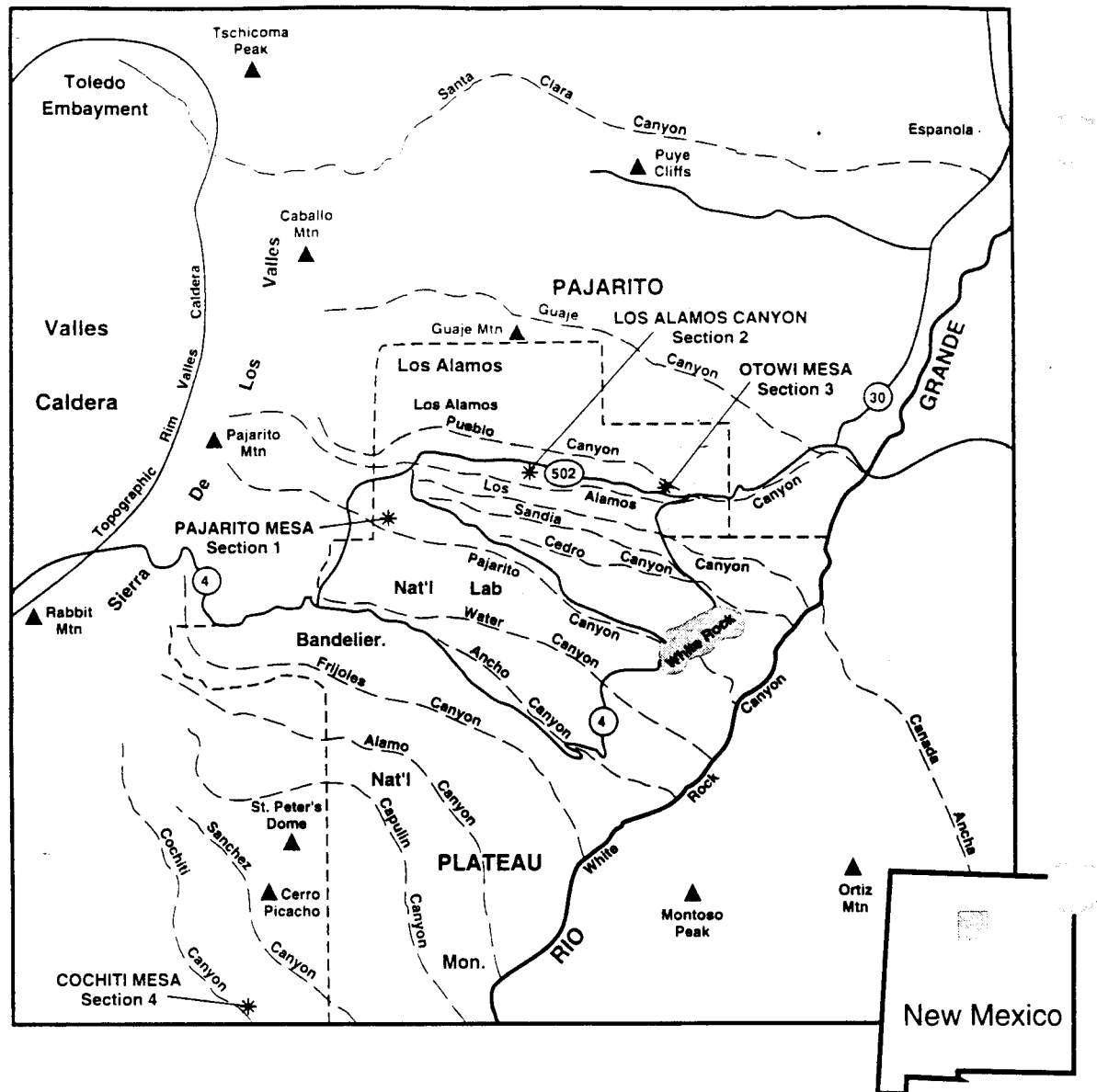


Fig. 1. Sample location map of the Pajarito Plateau, Jemez Mountains, New Mexico. Samples are from sections measured at Pajarito Mesa (Broxton, unpubl. data), Los Alamos Canyon (Broxton et al., 1995), Otowi Mesa (section 27 of Balsley, 1988) and Cochiti Mesa (section 20 of Balsley, 1988).

of 400 km³ dense rock equivalent (DRE), and is glassy and poorly to non-welded over much of the Pajarito Plateau (Fig. 1). At 1.22 million years (Izett and Obradovich, 1994), the Tshirege Member was erupted to form the Valles caldera at approximately

the same location as the earlier Toledo caldera (Self et al., 1986). The Tshirege Member is a non-densely welded compound cooling unit of some 150 to 300 km³ DRE, with no significant internal erosional breaks (Smith and Bailey, 1966; Crowe et al.,

1978; Fisher, 1979; Broxton et al., 1995). The character of the flow units varies markedly from surge-like to massive, structureless ignimbrite, and in places shows a number of welding reversals, attributed to cooling intervals between the emplacement of successive flow units (Smith and Bailey, 1966; Fisher, 1979; Self et al., 1986; Broxton et al., 1995). For simplicity, we will informally refer to the Otowi

Member as the Lower Bandelier Tuff (LBT) and the Tshirege Member as the Upper Bandelier Tuff (UBT) in the remainder of this paper. In both members, magmatic chemical and mineralogical variations are preserved in individual pumice fragments: systematic vertical chemical zonation is moderately well-preserved through the thickness of the UBT on the Pajarito Plateau (Smith and Bailey, 1966; Kuentz, 1986; Balsley, 1988; Warsaw and Smith, 1988; Caress, 1994; Broxton et al., 1995).

The stratigraphy of the UBT has been described by Smith and Bailey (1966), Bailey et al. (1969), Crowe et al. (1978), Vaniman and Wohletz (1990) and Broxton and Reneau (1995). Most of the proposed stratigraphic subdivisions of the UBT are based on the occurrence of surge beds and reversals in welding, but no single nomenclature has gained universal acceptance. For the purposes of this study, the most significant internal contact is between the glassy lower portion, and the massively devitrified upper portion of the unit. This contact is commonly marked by a persistent zone of differential weathering informally called the "vapor-phase notch".

The UBT is stratigraphically zoned from high-silica rhyolite (76–77 wt.% SiO₂) at its base to low-silica rhyolite (72 wt.% SiO₂) at its top, both in bulk-rock composition, and dominant pumice fragment composition (Smith and Bailey, 1966). However, low-silica rhyolite pumice fragments (increasingly abundant with stratigraphic height) and distinctive hornblende-dacite pumice fragments (< 1–5 vol.% throughout) appear to be present throughout (Fig. 2). Overall, chemical and mineralogical zonations of the dominant rhyolite magma, summarized in Fig. 3, are consistent with progressively deeper tapping of a zoned magma body throughout the eruption (Smith, 1979; Balsley, 1988; Caress, 1994). Recharge-related mixing (Stimac, in press) and eruptive drawdown effects (Blake and Ivey, 1986) are probably responsible for the co-eruption of different magmas from different levels of the chamber.

PHENOCRYST ASSEMBLAGES AND OCCURRENCE OF THE MAJOR COMPONENTS OF THE UPPER BANDELIER TUFF

SUBUNIT	LSR	CSX	HBD
4	↑ anorth cpx opx mag ilm zircon chev apatite monazite	↑ plag anorth Na-san cpx opx mag ilm apatite zircon	↑ plag hbd (cpx) (opx) mag ilm po apatite
3			
2			
1v	Na-san qtz cpx mag fay chev zircon apatite monazite		
vpn			
1g			
TP	↓		↓
	HSR		

Fig. 2. Phenocryst assemblages and occurrence of the major components of the Tshirege Member of the Bandelier Tuff (UBT). Stratigraphic subunits follow Broxton and Reneau (1995). TP is the Tsankawi Pumice Bed and vpn is the vapor-phase notch (see text). Major components of the UBT eruption include high-silica rhyolite (HSR), low-silica rhyolite (LSR), and hornblende-dacite pumice fragments (HBD), as well as cognate syenitic xenolithic debris (CSX).

4. Results and interpretation

4.1. Samples and stratigraphic zonation

We sampled four sections on the Pajarito Plateau (Pajarito Mesa, Los Alamos Canyon, Otowi Mesa

COMPOSITIONAL AND MINERALOGICAL ZONING	72 wt% SiO ₂		Bulk Composition		77 wt% SiO ₂	
	850 C		T: C		700 C	
	Or _{<5} ?		Or ₂₅		Or ₃₈ Or ₄₄	
	Plagioclase		Anorthoclase		Na-sanidine	
	En ₃₇ Fs ₂₂				En ₈ Fs ₄₉	
	Augite		CPX		Ferrohedenburgite	
	En ₅₂ Fs ₄₅				En ₂₅ Fs ₆₆	
	OPX		Hypersthene			
			F ₀₉		Quartz F ₀₃	
	Usp ₃₆				Fayalite Usp ₂₆	
	Ilm ₈₉		Ilm ₉₁		Magnetite	
	Ilmenite				Chevkinite	
					Zircon	
					Apatite	
				Monazite		
5	4	Smith and Bailey et al. (1966)		2	1	
4	3	Broxton and Reneau (1995)		17	19	
					TP	

Fig. 3. Mineral compositions of the major high-silica to low-silica rhyolite component of the UBT (data from Smith and Bailey, 1966; Warsaw and Smith, 1988; Caress, 1994; Stimac, unpubl. data; Werner and Hickmott, unpubl. data). Stratigraphic nomenclature of Caress and Bailey (1966) shown for comparison. Mineral abbreviations are: *anorth* = anorthoclase; *cpx* = clinopyroxene; *opx* = orthopyroxene; *mt* = magnetite; *ilm* = ilmenite; *chev* = chevkinite; *plag* = plagioclase; *Na-san* = sodic sanidine; *qtz* = quartz; *fay* = fayalite; *hbd* = hornblende; *po* = pyrrhotite; *En* = enstatite; *Fo* = forsterite; *Or* = orthoclase; *Fs* = ferrosilite; *usj* = ulvöspinel.

and Cochiti Canyon; Fig. 1) which together provide nearly complete exposures of both the LBT and UBT. In these sections, the LBT is glassy and non- to poorly welded throughout, whereas the UBT has a non-welded to incipiently welded, glassy base and non- to moderately welded devitrified top. Although the LBT was sampled, we concentrated on the UBT because previous investigations of it have been instrumental in the development of many concepts regarding ash flow eruption and emplacement, including zonal variations in ignimbrites (Smith, 1960; Ross and Smith, 1961).

In three of our four sections, the glassy lower portion of the UBT is separated from the overlying, massively devitrified portion by the earlier-men-

tioned vapor-phase notch (Fig. 4). Below this zone XRD analysis cannot quantify trace-mineral abundances because they typically comprise < 2% of the rock, however, just below the vapor-phase notch cristobalite becomes measureable (Fig. 4). Portions of the UBT above the vapor-phase notch show both axiolitic crystallization of shards to cristobalite and alkali feldspar (devitrification), and vapor-phase crystallization of tridymite, alkali feldspar and lesser cristobalite, primarily in pumice fragments. The highest cristobalite content occurs just above the vapor-phase notch, in non-welded to poorly welded tuff dominated by axiolitic crystallization. At higher stratigraphic levels tridymite and alkali feldspar become dominant, primarily due to growth during va-

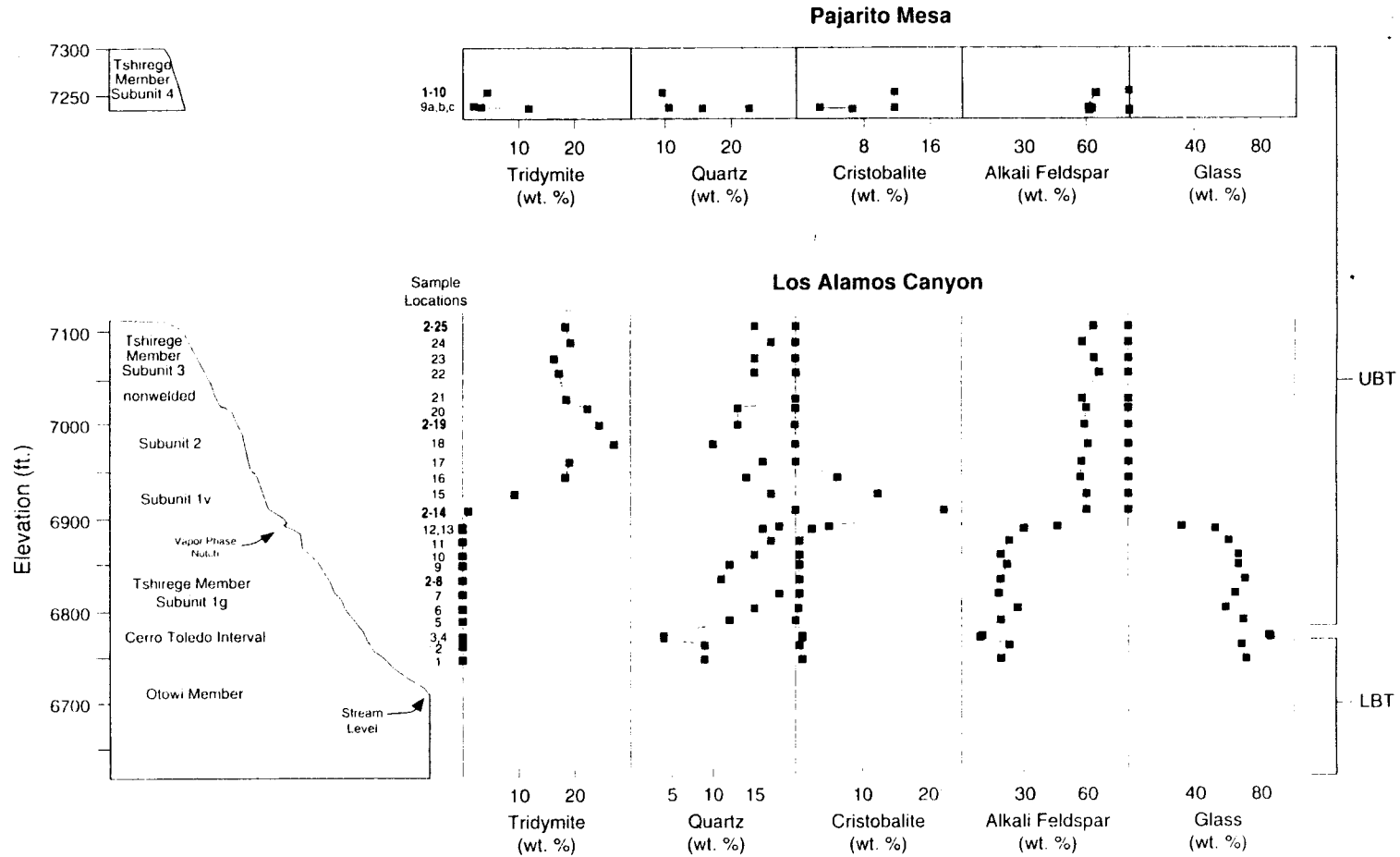


Fig. 4. Composite stratigraphic section and major mineralogy of the Bandelier Tuff based on measured sections at Los Alamos Canyon and Pajarito Mesa by Broxton et al. (1995) and Broxton (unpubl. data) using the nomenclature of Broxton and Reneau (1995). Quantitative X-ray diffraction data for minerals (glass by difference) are plotted versus stratigraphic position (Bish and Chipera, 1988). Samples examined in this study are shown in bold (see Table 1 for whole-rock data).

por-phase crystallization of pumice fragments in the more densely-welded portion of the unit (Fig. 4). In the most affected zones, thick vapor-phase overgrowths were formed on alkali feldspar and FeTi-oxide phenocrysts.

The fourth section, originally measured at Cochiti Mesa by Balsley (1988), is along a paleocanyon-wall contact and provides glassy samples of stratigraphic levels that are devitrified in the other UBT sections. This section appears to have been variably affected by focusing of vapor along a relatively impermeable contact with older dacitic and andesitic lavas. This is evidenced by the presence of fossil fumarolic pipes, vapor-phase crystallization in pores, and local bleaching and variegated coloration in shades of red, red-brown, yellow and orange. As shown later, some samples from this section have Pb concentrations an order of magnitude higher than those in other sections. Fossil fumarolic pipes are also present toward the top of the Pajarito Mesa section, but were not observed in the other sections. Fracture mineralogy has not been studied for all sections, however, fractures near the Pajarito Mesa section are reddened by hematite accumulation, probably from vapor alteration. Later fracture fillings include halite (up to 10 wt.%), lesser gypsum and abundant detrital clay coatings (Vaniman and Chipera, unpubl. Los Alamos National Lab report).

4.2. Pre-eruptive mineralogy and chemistry

In order to understand the mineral assemblages formed during eruption and devitrification of the UBT, it is important to first document the mineralogical and chemical variations present in the parent magma body. As shown in Fig. 2, our work suggests that the pre-eruptive mineralogy of the UBT included contributions from at least three distinct sources: (1) minerals that grew from the dominant high-silica (HSR) to low-silica rhyolite (LSR) magma; (2) minerals included within, or derived from disaggregated hornblende-dacite (HBD) pumice fragments (Stimac, in press); and (3) minerals making up, or derived from cognate syenitic xenoliths (CSX). This xenolithic debris is present only in the later erupted material (Warshaw and Smith, 1988; Caress, 1994), and is thought to represent cognate chamber wall material (Fig. 2). Despite this com-

plexity, it is important to note that rhyolitic glass (or crystalline equivalent), alkali feldspar (Or_{44-25}) quartz phenocrysts compose 96–99 vol.% of the juvenile component of the unit.

Our chemical data for glassy pumice fragments, glassy and devitrified bulk tuff, and matrix glass from the UBT, combined with published chemical data, show systematic enrichment of incompatible trace elements downwards in the ignimbrite (Table 1; Fig. 5). This accords with the observation that the upper parts of silicic magma bodies are commonly enriched in volatiles and incompatible trace elements, and that ash-flow tuffs crudely preserve inverted versions of this zonation (e.g., Lipman et al., 1966; Smith, 1979; Hildreth, 1981). This trend of enrichment is best seen in variation diagrams of two highly incompatible elements such as Rb and Nb (Fig. 5A). These elements define linear trends, with the slope being a measure of their relative incompatibility. Simple crystal fractionation models assuming subtraction of observed mineral assemblages and proportions generally account for the observed trends (Fig. 5A; Balsley, 1988; Stix et al., 1988).

The extreme and non-linear variability of some elements (Pb, As, Sb) cannot be explained by crystal fractionation (Fig. 5B). For example, crystal fractionation models generally account for the main trend of Pb data (Fig. 5B), but not the sporadic high Pb concentrations > 50 ppm. Based on studies of magmatic volatiles and fumarolic assemblages (e.g., Symonds and Reed, 1993) and mineralogical evidence presented below, we propose that in the Bandelier system Pb was among the most mobile elements in magmatic vapor and in vapor liberated during devitrification, and thus its variability in part reflects syn- to post-emplacement redistribution processes.

4.3. Syn- and post-eruptive mineralogy

In seminal works on zonal variations in ash-flow tuffs, Smith (1960) and Ross and Smith (1961) drew clear distinctions between *devitrification*, *vapor-phase crystallization* and *fumarolic alteration*. They restricted *devitrification* to growth of spherulitic and axiolitic intergrowths of cristobalite and alkali feldspar (plus minor accessory minerals) from massive glass, whereas they referred to *vapor-phase*

crystallization as growth of crystals (mainly alkali feldspar, cristobalite and tridymite) from a vapor, in pore spaces. They noted that the products of vapor-phase crystallization are generally coarser-grained, and form during and after devitrification. The gen-

eral distribution of vapor-phase crystallization is controlled by the distribution of pore space and trapped gas in the unit. Smith (1960) considered *fumarolic alteration* to be distinct from, but transitional to, vapor-phase crystallization, arguing that fumarolic

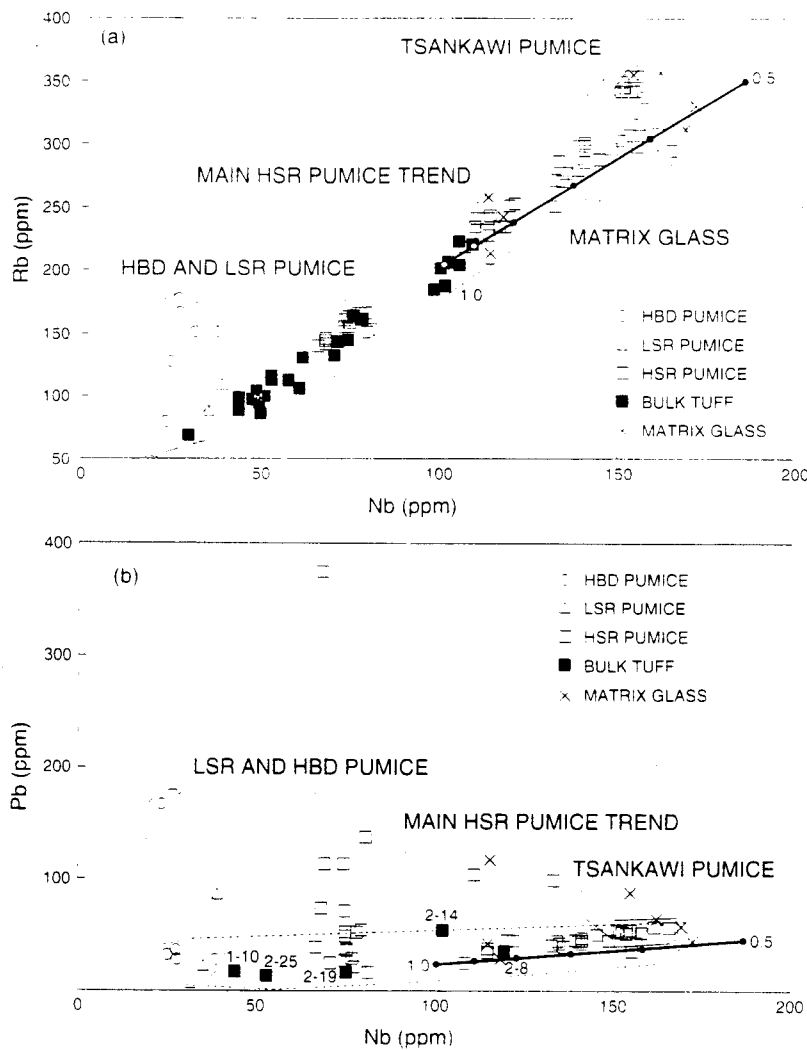


Fig. 5. Trace-element variation for bulk tuff, glassy pumice fragments, and matrix glass determined by XRF, GFAA and PIXE (data from Balsley, 1988; Stix et al., 1988, Table 1/ Table 4/ Table 5). (A) Rb versus Nb for pumice fragments, bulk tuff, and matrix glass (abbreviations same as in Fig. 2). Line indicates the Rayleigh fractionation trend for the observed mineral assemblage in the first erupted Tshirege Member of the Bandelier Tuff (UBT) assuming bulk $D_{\text{Nb}} = 0.094$ and $D_{\text{Rb}} = 0.171$; dots along the line indicate fraction of liquid remaining. Partition coefficients for all phases determined by PIXE analyses of minerals and glass, with bulk distribution coefficients calculated from observed modal proportions. (B) Pb versus Nb for pumice fragments, bulk tuff, and matrix glass. Pb concentrations in bulk tuff samples from the major subunits of the UBT generally decline from bottom to top of the UBT, with the exception of sample 2-14, which has the highest Pb and Zn concentrations. Glassy pumice fragments with the highest Pb concentrations are from the Cochiti Mesa section. Line indicates Rayleigh fractionation trend assuming bulk $D_{\text{Nb}} = 0.094$ and $D_{\text{Pb}} = 0.173$; dots along line indicate fraction of liquid remaining.

Table 1
Whole-rock chemical data for selected UBT samples

Sample:	2-8 glassy	2-14 devitrified	2-19 devitrified	2-25 devitrified	1-10 devitrified
Subunit:	1g	1v	2	3	4
<i>XRF data</i>					
SiO ₂ (wt.%)	77.34	77.18	77.68	76.43	74.41
TiO ₂	0.08	0.09	0.09	0.12	0.24
Al ₂ O ₃	12.05	11.93	11.87	12.49	13.16
Fe ₂ O ₃	1.57	1.48	1.50	1.65	2.28
MnO	0.08	0.08	0.06	0.06	0.07
MgO	< 0.06	< 0.06	< 0.06	< 0.06	0.16
CaO	0.28	0.16	0.21	0.36	0.50
Na ₂ O	4.05	4.03	4.13	4.10	4.43
K ₂ O	4.53	4.37	4.49	4.57	4.73
P ₂ O ₅	< 0.01	0.01	< 0.01	< 0.01	0.02
Rb (ppm)	234	187	145	116	89
Sr	16	27	16	28	58
Y	88	92	34	46	29
Zr	222	204	208	247	353
Nb	119	102	75	53	44
Ba	83	112	65	165	324
<i>GFAA data</i>					
Pb (ppm)	34	55	17	14	17
Zn	96	106	66	50	59
Cu	2	4	2	4	5
Ni	< 1	< 1	< 1	5	5
Mo	2.9	< 1	< 1	< 1	< 1
Cr	6	6	8	11	9
Co	16	16	14	15	26

All analyses are for bulk tuff. Major elements normalized to 100%, volatile free; total Fe as Fe₂O₃. Sample locations and stratigraphic positions shown in Fig. 4. XRF = X-ray fluorescence analysis. GFAA = graphite-furnace atomic-absorption analysis. See Section 2 for details of analysis procedures.

alteration products form mainly at lower temperatures. Although fossil fumaroles are generally less obvious than in younger deposits such as Crater Lake, Oregon or Valley of Ten Thousand Smokes, Alaska (Ross and Smith, 1961), locally dense populations occur, both at the top of the glassy portion, and near the top of the devitrified portion of the UBT (e.g., Crowe et al., 1978).

In our study of the Bandelier Tuff, we have documented the assemblages of accessory minerals that formed: (1) directly from trapped or exsolving magmatic vapor; (2) from vapor liberated through post-emplacement crystallization of glass; and (3) by reaction of vapor with existing phenocrysts. Thus,

the syn- to post-eruptive mineral assemblages span the full range of devitrification, vapor-phase crystallization, and fumarolic alteration as envisioned by Smith (1960). These assemblages may be especially diverse in the Bandelier Tuff because it is poorly to non-welded in most outcrops, which allowed relatively free travel of vapor throughout. In addition to this high permeability, factors such as the amount of precipitation and direction of groundwater flow, must also have contributed to the extent and directions of vapor transport in the UBT (Goff and Shevenell, pers. commun., 1995).

Like earlier workers, we were unable to document the devitrification mineral assemblage making up axiolitic intergrowths beyond alkali feldspar and

Table 2
Vapor-phase and replacement minerals in UBT samples

Sample	Vapor-phase minerals	Replacement minerals
<i>UBT — Cochiti Mesa Section</i>		
20-70 (glassy)	magnetite [Fe ₃ O ₄] (Cu,Ag) ₂ S, cerargyrite? [AgCl] monazite WO ₃	none observed
20-63 (glassy)	magnetite FeS ₂ (Ni,Cu,Ag,Fe)S, (Pb,V,Ca,K)O ₂	none observed
20-22 (glassy)	magnetite (tabular) barite (Sn,Fe) ₂ O ₇	none observed
<i>UBT — Los Alamos Canyon and Pajarito Mesa sections</i>		
1-10 (devitrified)	magnetite	smectite, hematite
2-25 (devitrified)	magnetite galena [PbS] Pb(CO ₃) BiCl apatite [Ca ₅ (PO ₄) ₃ OH.F.Cl]	smectite illite/sericite?
2-19 (devitrified)	magnetite titanite [CaTi(SiO ₄)O.OH.F] sylvite [KCl]	smectite hematite illite/sericite?
2-14 (devitrified)	magnetite zircon monazite Nb,Y,Fe oxide?	smectite hematite
2-8 (glassy)	magnetite	none observed

Samples listed in stratigraphic order; all devitrified samples are dominated by alkali feldspar and tridymite ± cristobalite.

cristobalite, because it is too fine-grained to analyze by conventional techniques. Vapor-phase minerals in the UBT consist dominantly (> 99 vol.%) of alkali feldspar, cristobalite, tridymite and magnetite (Table 2); however, a diverse suite of other minerals is present at trace abundances (< 1 vol.%). These minerals occur as euhedral to subhedral crystals and

intergrowths both on vesicle surfaces in glassy samples (Fig. 6A), and on the grain surfaces and boundaries making up the dominant vapor-phase assemblage in devitrified samples (Fig. 6B).

We confirmed the presence of vapor-phase magnetite, zircon, titanite, monazite, apatite, sylvite, barite and unidentified minerals rich in Ba, Nb, Y

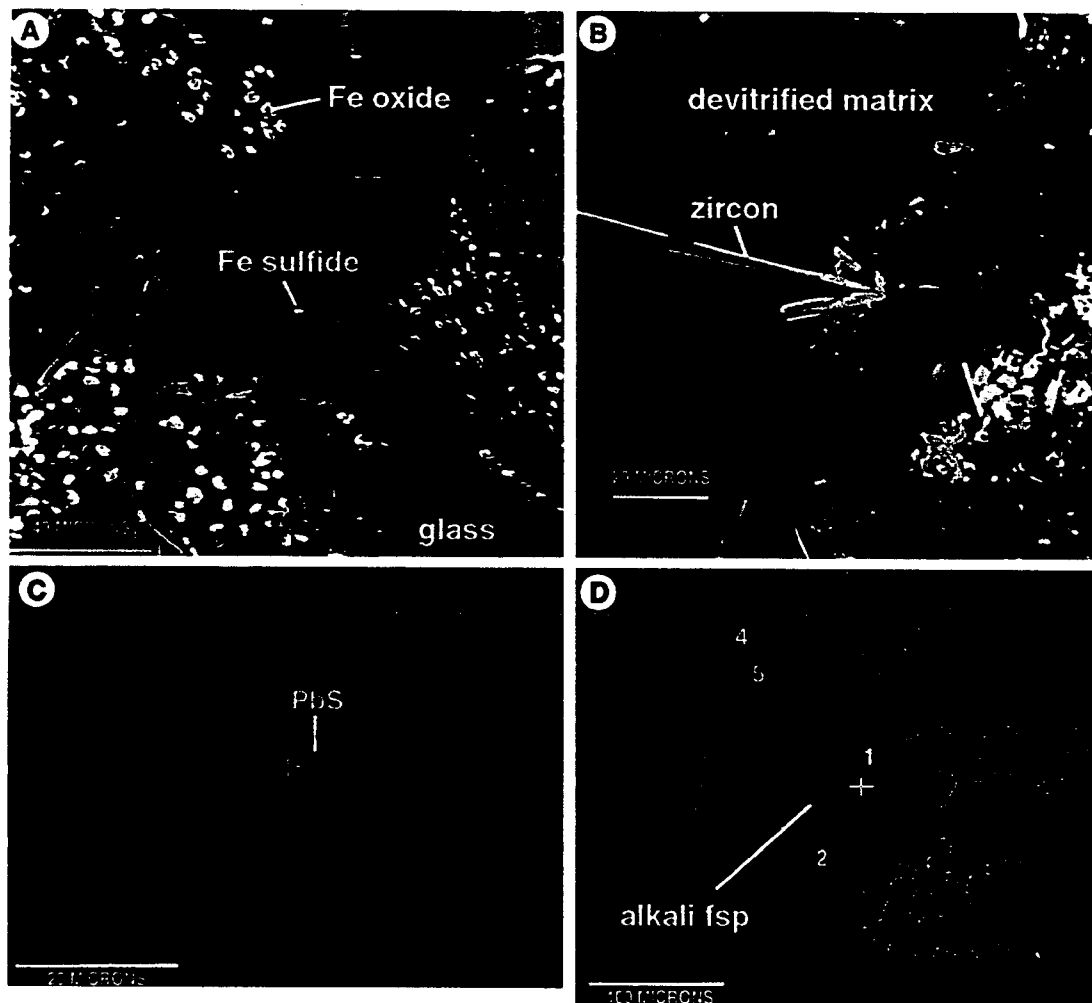


Fig. 6. Backscattered-electron images of vapor-phase mineral and glass textures in the Tshirege Member of the Bandelier Tuff (UBT). (A) Very fine-grained *Fe oxide* and *Fe sulfide* (labelled) grains on a glassy substrate (broken chip of sample from Cochiti Mesa section). (B) Zircon needles on the surface of devitrified tuff (broken chip of sample 2-14). Such acicular *zircon* is abundant in this sample, which also has the highest cristobalite content (Fig. 4). (C) Polished thin section of devitrified tuff, consisting mainly of alkali feldspar and tridymite (medium grays), and Fe-oxide (white) in sample 2-25. A subhedral crystal of *PbS* (labelled) is on the surface of a tridymite grain. Crystal shape and location indicate that the galena grew from vapor during crystallization of the tuff. (D) Polished thin section of devitrified tuff with cristobalite (darkest gray, with polygonal cracking) and K- and Fe-rich vapor-phase alkali feldspar (*alkali fsp*) overgrowths on Na-sanidine phenocryst (light-gray rims, medium-gray grains). Labelled points indicate sites of PIXE analyses plotted in Fig. 8 and Fig. 9.

and/or LREE (Table 2). We also documented the occurrence of phases containing Pb, Bi, Fe, Ag, Cu, Zn, V, Ni, W and Sn (Fig. 6). For the most part, the latter phases were identified as either sulfides, sulfates, chlorides, phosphates, or were presumed to be oxides, hydroxides, or carbonates because other anions such as S or Cl were absent. The most common Pb mineral identified was galena (Fig. 6C), but a variety of other Pb-bearing phases were observed. Perhaps the most unusual phase we identified was a Pb carbonate in a glassy LBT sample, containing up to 6 wt.% Ag and 1–2 wt.% Re as determined by WDS analysis. This glassy sample also contained an unusual abundance of other trace-metal-rich minerals including galena, sphalerite and lead-antimony sulfide, but lacked the most common products of devitrification and vapor-phase crystallization (alkali feldspar, tridymite and cristobalite). Although numerous trace phases were observed, we suspect further examination would yield an even wider array of minerals, especially lower atomic-number minerals that were not specifically targeted in this study.

Although most trace-mineral grains appear to have grown randomly from vapor in pore spaces, some mineral growth was localized by phenocrysts. For example, alkali feldspar phenocrysts, typically ranging in composition from Or_{44-25} , commonly have more potassic and Fe-rich overgrowths (Fig. 6D), whereas mafic silicates and FeTi-oxide phenocrysts host a variety of vapor-phase minerals and alteration products (Fig. 7). An alteration assemblage of smectite and hematite \pm micron-scale vapor-phase minerals commonly replaces or partially replaces pyroxene and fayalite grains (Fig. 7A). This assemblage is absent in glassy samples, but ubiquitous in devitrified portions of the UBT, indicating that replacement occurred during post-emplacement crystallization and

cooling of the unit. This interpretation is in accord with the observations that: (1) mafic silicates are typically pristine in glassy lavas and tuffs, but are pervasively replaced by clay minerals and Fe-oxides in devitrified equivalents (e.g., Ross and Smith, 1961); and that (2) similar alteration of mafic silicates and plagioclase has been described by Keith (1991) and Spilde et al. (1993) adjacent to fossil fumaroles from the Valley of Ten Thousand Smokes (VTTS), Alaska.

Mineral assemblages and textures surrounding mafic silicates are complex and deserve further study. Smectite and Fe-oxides form numerous layers separated by open space, suggesting multiple pulses of deposition (Fig. 7A and B). Magmatic accessory minerals (such as zircon and chevkinite) that were present as inclusions in pyroxene and fayalite phenocrysts commonly are preserved despite complete replacement of the host mineral. Magnetite (originally included within or on the surfaces of pyroxene) is exsolved, and displays a wide range of surface textures. Some magnetite grains have subhedral surfaces (Fig. 7B and C), whereas others are overgrown by rosettes of Fe-oxide with lower Ti content, probably hematite (Fig. 7D). Rietveld XRD analyses of magnetic mineral concentrates from samples of devitrified UBT have shown that hematite ranges from 9 wt.% of the total, and that magnetite is variably oxidized to maghemite. Unidentified Pb minerals are also present as trace constituents of the alteration assemblage (Fig. 7E).

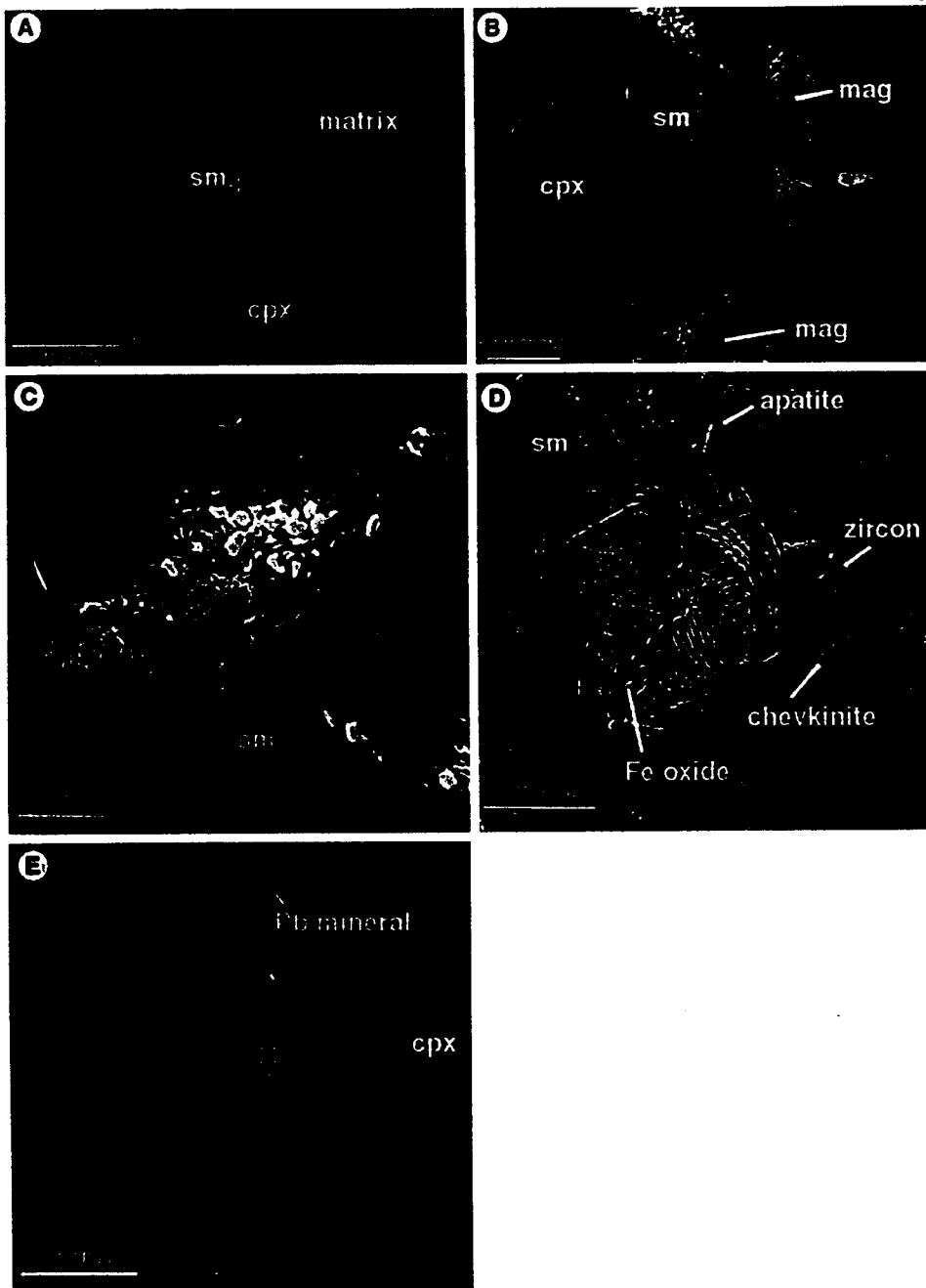
4.4. Pb concentrations of minerals and glass

Pb concentrations of minerals, glass, and devitrified matrix determined by PIXE are plotted versus Fe concentrations in Fig. 8 (see Tables 3–5 for

Fig. 7. Backscattered-electron images of alteration products associated with pyroxene and Fe-Ti-oxide phenocrysts in devitrified samples. (A) Polished thin section of clinopyroxene (*cpx*) phenocryst (medium gray), partially replaced by layers of iron-rich smectite (*sm*: light gray to white) in sample 2-14. (B) Broken chip of sample of single, partially replaced clinopyroxene phenocryst with adhering magnetite phenocrysts. The scalloped surface of the clinopyroxene is coated by layered, porous smectite-hematite intergrowths (*sm*) in sample 2-14. Magnetite phenocrysts (*mag*) have subhedral shapes indicating that they retained their original crystal outlines, or were the sites of additional vapor-phase growth. (C) Broken chip of sample of magnetite with a pitted, subhedral surface, hosting numerous grains of monazite, and an unidentified Nb-Y-Fe mineral. (D) Broken chip of sample of Fe-oxide rosette (probably hematite) on surface of smectite (sample 2-14). Numerous *apatite*, *zircon* and *chevkinite* grains surround the rosette. These grains are probably accessory microphenocrysts that were originally included in the pyroxene, but some may have formed or seen additional growth during vapor-phase crystallization. (E) Polished grain mount with cavity in partially replaced clinopyroxene (*cpx*), containing a variety of minerals including apatite, smectite, hematite, and an unidentified *Pb* phase, probably Pb oxide or carbonate (sample 2-25).

representative analyses). Glass has highly variable, but higher Pb concentrations (29–118 ppm) than any major phenocryst phase, including alkali feldspar (< 7–22 ppm). PIXE analyses of coexisting glass

and alkali feldspar yield apparent mineral/melt partition coefficients (concentration of Pb in mineral/concentration of Pb in matrix glass) averaging about 0.3. Unaltered mafic silicates and FeTi-



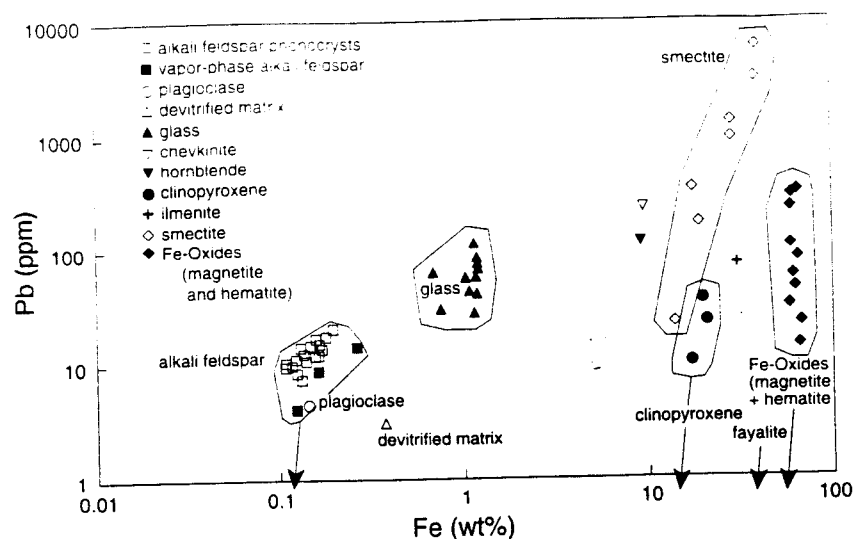


Fig. 8. Pb (ppm) determined by PIXE versus Fe (wt%) determined by EMP for minerals, glass, and matrix for the Tshirege Member of the Bandelier Tuff (UBT). Arrows indicate that some mineral grains have Pb concentrations below detection by PIXE.

oxides from glassy samples generally have Pb concentrations below detection (about 7 ppm for typical analyses), whereas partially replaced grains of these same minerals from devitrified samples display a wide range of higher Pb concentrations (< 7 to over 100 ppm), overlapping with the range exhibited by the associated alteration assemblage. Direct analyses of replacement products (dominantly smectite and hematite) of mafic silicates yielded semi-quantitative results due to the problems of analyzing porous, fine-grained mixtures of minerals; however, these mixtures clearly have higher Pb contents than those of any other analyzed material, as indicated by the prominent Pb peaks in PIXE-EDS spectra (see Table 4 for representative analyses). SEM images show that these alteration assemblages are commonly the sites of micron-scale vapor-phase crystallization that includes Pb minerals (Fig. 7E). However, it is possible that reactive surfaces of these minerals also sorbed Pb, as indicated by high Pb concentrations in clay minerals and Fe-oxides in soils (e.g., Soldatini et al., 1976; Farrah and Pickering, 1977), and relatively uniform Pb distributions as determined by time-of-flight secondary-ion mass spectrometry (SIMS) imaging analysis of our samples (Mogk, pers. commun., 1995).

Vapor-phase alkali feldspars and devitrified ma-

trix apparently have lower Pb concentrations than phenocrysts (Fig. 9), but data for the vapor-phase feldspars and matrix must be viewed as semi-quantitative, due both to their fine grain size relative to the PIXE beam, and their low Pb concentrations (near detection limit by PIXE).

5. Discussion

Our study of the Bandelier Tuff indicates that some redistribution of trace metals such as Pb occurred during eruption, post-emplacment crystallization, and cooling of the unit. In the following sections we will discuss redistribution that occurred during eruption separately from redistribution that occurred during subsequent devitrification, vapor-phase crystallization, and cooling. Making this distinction is important because more detailed study of eruptive metal fluxes is needed to better estimate the contribution of volcanoes to global metal budgets (e.g., Nriagu, 1989).

5.1. Pre- and syn-eruptive partitioning of metals

Discussion of eruptive metal losses involves determination of metal concentrations in silicate melt.

Table 3
Selected electron microprobe and quantitative PIXE data for phenocryst minerals and glass

Mineral: PIXE P.T.:	Glass			Phenocrysts									
	GL(m)	GL(m)	GL(i)	PLAG	SAN	SAN	SAN	CPX	CPX	FAY	HB	ILM	MAG
Sample:	1226	1346	1253	1381	1227	1241	1342	1221	1370	1356	1312	1257	1357
	2-8	2-8	2-14	2-7(HBD)	2-8	2-25	2-8	2-8	2-14	2-8	2-7(HDP)	2-14	2-8
SiO ₂ (wt.%)	74.02	74.51	74.66	58.90	66.95	67.31	68.05	48.52	49.48	29.38	43.32	0.11	0.12
TiO ₂	0.05	0.10	0.05	-	-	-	-	0.13	0.15	0.01	2.74	42.24	9.94
Al ₂ O ₃	11.55	11.87	11.62	24.79	18.89	18.99	19.00	0.26	0.29	0.02	11.24	0.03	0.45
FeO	1.48	1.50	1.35	0.19	0.21	0.17	0.25	27.43	25.34	62.19	12.05	38.84	82.45
MnO	0.08	0.10	0.07	-	-	-	-	2.55	2.04	5.08	0.15	12.74	1.18
MgO	< 0.01	0.01	< 0.01	-	-	-	-	2.20	3.73	1.97	13.22	0.14	0.12
CaO	0.22	0.24	0.26	6.80	0.12	0.33	0.15	17.38	18.16	0.19	10.94	-	-
Na ₂ O	4.09	4.18	4.00	7.35	6.68	6.57	6.76	0.66	0.54	0.03	2.21	-	-
K ₂ O	4.22	4.57	4.58	0.58	7.44	6.85	7.44	-	-	-	-	-	-
Total	95.71	97.08	96.59	98.61	100.28	100.22	101.65	99.13	99.73	99.37	95.87	94.10	94.26
Fe (ppm)	11426 (72)	11660 (78)	10494 (76)	1477 (10)	1632 (12)	1321 (10)	1943 (13)	203577 (4379)	196970 (5467)	483409 (10487)	93004 (2149)	301907 (8481)	640867 (15917)
Cu	36 (5)	ND	29 (5)	ND	5 (1)	3 (1)	ND	ND	ND	ND	ND	ND	ND
Zn	169 (5)	164 (2)	164 (6)	5 (1)	6 (1)	3 (1)	6 (1)	961 (16)	851 (26)	2021 (32)	116 (8)	2202 (63)	2932 (57)
Ga	40 (3)	33 (1)	39 (3)	18 (< 1)	38 (1)	26 (1)	43 (1)	11 (3)	ND	ND	25 (3)	ND	75 (8)
Ge	10 (2)	5 (1)	12 (3)	1 (< 1)	4 (1)	2 (< 1)	3 (1)	15 (2)	ND	ND	ND	ND	ND
Rb	329 (12)	356 (6)	290 (13)	3 (1)	111 (3)	41 (2)	133 (3)	ND	ND	ND	ND	87 (7)	ND
Sr	ND	ND	ND	592 (8)	ND	49 (4)	12 (3)	ND	ND	ND	224 (4)	ND	ND
Y	94 (8)	111 (4)	99 (8)	2 (< 1)	ND	ND	ND	339 (3)	345 (7)	40 (2)	40 (2)	70 (7)	392 (5)
Zr	322 (11)	300 (4)	269 (11)	20 (2)	ND	ND	ND	81 (2)	55 (3)	ND	55 (3)	422 (13)	4550 (18)
Nb	172 (9)	162 (4)	154 (9)	ND	ND	ND	ND	ND	ND	20 (1)	6 (2)	3734 (36)	617 (7)
Mo	16 (5)	ND	20 (6)	ND	ND	ND	ND	ND	ND	ND	ND	24 (7)	140 (8)
Pb	43 (7)	63 (3)	58 (8)	4 (1)	16 (2)	11 (1)	21 (2)	ND	37 (7)	ND	119 (6)	74 (14)	ND
Th	37 (8)	59 (4)	47 (10)	ND	ND	ND	ND	14 (3)	ND	12 (3)	ND	ND	44 (7)
U	ND	14 (4)	ND	5 (1)	ND	ND	ND	ND	ND	ND	ND	ND	ND

GL = glass; (m) = matrix; (i) = inclusion; SAN = sodic sanidine; PLAG = plagioclase; CPX = clinopyroxene; HB = hornblende; FAY = fayalite; ILM = ilmenite; MAG = magnetite; HBD = hornblende dacite pumice; ND = not detected by PIXE analysis; - = not analyzed. Major element oxides by electron microprobe (EMP) with total Fe expressed as FeO. Trace elements by PIXE except Fe (by EMP). 1-sigma counting statistic errors in parentheses. See Section 2 for details of analysis procedures.

Table 4
Selected electron-microprobe and semi-quantitative PIXE data for vapor-phase and replacement minerals

Point: Sample:	Alkali feldspar		Matrix	Matrix	Exsolved Fe oxides		Smectite	
	1363 2-14	1364 2-14	1368 2-25	1249 2-14	1306 2-19	1308 2-25	1256 2-14	1414 1-10
SiO ₂ (wt.%)	68.16	67.14	66.74	78.97	0.74	0.05	23.96	40.22
TiO ₂	0.00	0.00	0.00	0.03	8.42	9.59	0.15	0.16
Al ₂ O ₃	18.88	17.52	17.15	7.38	0.27	0.28	4.81	4.59
FeO	0.21	0.16	0.48	0.34	80.61	80.65	36.31	21.53
MnO	0.00	0.00	0.00	0.02	1.28	0.24	2.13	1.93
MgO	0.00	0.00	0.00	< 0.01	0.05	0.02	1.17	2.59
CaO	0.01	0.01	0.01	0.03	0.01	0.01	3.29	1.41
Na ₂ O	3.92	4.09	4.32	2.20	–	–	0.17	0.05
K ₂ O	9.99	10.24	9.74	3.63	–	–	0.33	0.85
Total	101.17	99.16	98.44	92.60	91.38	90.84	72.32	73.33
Fe (ppm)	1632 (10)	1244 (7)	3731 (158)	2643 (17)	626590 (14930)	626900 (15003)	282241 (6168)	187798 (6246)
Cu	2 (< 1)	ND	ND	5 (1)	ND	ND	280 (74)	ND
Zn	12 (< 1)	11 (< 1)	24 (2)	20 (1)	6112 (131)	1623 (58)	1451 (41)	627 (39)
Ga	9 (< 1)	5 (< 1)	4 (1)	9 (1)	120 (25)	72 (15)	81 (11)	202 (20)
Ge	ND	ND	ND	2 (1)	ND	ND	ND	ND
Rb	124 (2)	51 (1)	12 (1)	140 (4)	432 (15)	ND	125 (6)	941 (19)
Sr	ND	ND	4 (< 1)	ND	33 (8)	31 (6)	26 (4)	173 (10)
Y	8 (1)	3 (1)	14 (1)	41 (2)	537 (18)	926 (16)	903 (14)	45 (13)
Zr	47 (1)	18 (1)	50 (1)	105 (3)	1082 (22)	3371 (30)	130 (7)	1464 (25)
Nb	14 (1)	7 (< 1)	3 (1)	75 (3)	4529 (45)	111 (10)	ND	167 (12)
Mo	ND	ND	ND	ND	ND	93 (10)	ND	ND
Pb	9 (1)	4 (< 1)	3 (1)	14 (2)	322 (26)	86 (15)	1317 (26)	173 (19)
Th	ND	4 (< 1)	ND	19 (2)	107 (26)	ND	75 (12)	ND
U	5 (1)	ND	ND	ND	ND	ND	32 (9)	ND

ND = not detected by PIXE analysis; – = not analyzed. Major-element oxides by electron microprobe (EMP) with all Fe expressed as FeO. Trace elements by PIXE except Fe, which is by EMP analysis. 1-sigma counting statistic errors in parentheses. See Section 2 for details of analysis procedures.

and coexisting volatile phases at the time of eruption. Macdonald et al. (1992) found Pb abundances in obsidians from continental interiors are highest and correlate ($r \geq 0.6$) with F, Be, Nb, Ta and Li, lithophile elements known to have an affinity for magmatic liquid and/or vapor (e.g., Webster and Duffield, 1991; Hinkley et al., 1994). Thus, it is not surprising that Pb is also concentrated toward the roofs of large silicic magma bodies, as evidenced by compositionally zoned ignimbrites such as the Bishop and Bandelier Tuffs (Hildreth, 1979; Balsley, 1988; Macdonald et al., 1992). In such systems, bulk distribution coefficients (D_{pb}) $\ll 1$ appear to reflect the incompatibility of Pb in common silicate minerals relative to silicate melt. This may be due in part to the abundance of volatiles including halogens in the evolved caps of silicic magma bodies, which may

enhance the stability of metals in the melt phase and/or coexisting volatile phases. Moreover, these effects may be strongest in chlorine-rich silicic magmas with peralkaline affinities (e.g., peralkaline and Fe-rich high-silica rhyolites such as the Bandelier Tuff), which have among the lowest sanidine D_{pb} measured (generally < 0.3).

It is not known whether there was a co-existing volatile phase in the UBT magma at the time of eruption (cf. Dunbar and Hervig, 1992), but in situ studies of melt and fluid inclusions from other systems have shown that pre-eruption contents of some metals in melts and fluid phases exceed those of "degassed" matrix glass (Lowenstern et al., 1991; Webster and Duffield, 1991; Bodnar et al., 1993; Lowenstern, 1993; Webster and Duffield, 1994). These results, along with evidence that the upper

portions of many silicic magma bodies are saturated with one or more volatile phase prior to eruption (Anderson, 1991; Dunbar and Hervig, 1992; Lowenstern, 1994; Wallace and Gerlach, 1994), indicates that a significant amount of volatile metals could be released to the atmosphere, or re-precipitated on tephra during eruption (Smith et al., 1982; Zoller et al., 1983).

The presence of Pb, Sb, Ag and Re-rich trace minerals in *glassy* samples of the LBT and UBT suggests that these minerals grew directly from pre- or syn-eruptive magmatic vapors. However, their very low modal abundance and sporadic distribution complicate any assessment of the extent of eruptive metal degassing. Neither are our PIXE data on melt

inclusions of sufficient quality and quantity to resolve this question. Further work using SIMS is planned to address this issue.

5.2. Post-eruptive redistribution of trace metals

Whereas some fraction of volatile trace elements may be released to the atmosphere during eruption, a much higher proportion remains in trapped gas and glassy tephra. Crystallization, cooling, and further degassing of an ash flow will continue to redistribute these volatile elements. Zielinski et al. (1977) showed that devitrified portions of lavas commonly have lower concentrations of volatile elements (Li, Sc, U, Mo and F), and higher concentrations of refractory elements (Sr, Ba and Eu) than associated obsidian, which they attributed to a combination of high-*T* (crystal-melt fractionation, volatile transport) and low-*T* (ion exchange, differential solution and adsorption by secondary phases) processes. A number of workers (e.g., Keith, 1991; Papike et al., 1991) have shown that metals, including Pb, are strongly concentrated in the upper portions of fossil fumarolic pipes in the VTTS, Alaska.

By knowing the Pb concentrations and the modal abundances of minerals in the UBT, we estimate that > 95% of Pb resided in the silicate liquid prior to eruption, and thus was susceptible to redistribution during eruption and post-emplacement crystallization and degassing. Because Pb is not strongly partitioned into any major phase during post-emplacement crystallization of glass, a high proportion of this Pb would have been available for local redistributed by vapor. However, the relatively systematic trends of most samples with stratigraphic position indicate that the original compositional zonation of Pb is largely preserved, and that only in areas of extensive vapor transport (e.g., impermeable contact along canyon walls) did significant mass transport of Pb occur on the scale of a hand sample. We have documented that some fraction of Pb was deposited in micron-scale minerals on surfaces. In devitrified samples, an even greater fraction of metals is likely to reside in sub-micron-scale minerals along grain boundaries of the dominant phases.

Our data for the UBT confirm that metals are present in a variety of acid-soluble sulfide and oxide minerals on ash surfaces, as previously suggested by

Table 5
Selected electron microprobe and quantitative PIXE data for trace minerals

Mineral	Zircon	Chevkinite
Point:	1297	1259
Sample:	1-10	2-14
SiO ₂	32.51	19.0
TiO ₂	0.00	13.45
ZrO ₂	67.02	–
Al ₂ O ₃	0.21	–
FeOT	0.08	12.27
Nb ₂ O ₅	–	3.76
CaO	0.22	2.35
Ce ₂ O ₃	–	21.11
La ₂ O ₃	–	11.36
Nd ₂ O ₃	–	6.05
Fe(ppm)	ND	95376 (5966)
Cu	ND	ND
Zn	ND	180 (48)
Ga	ND	ND
Ge	ND	ND
Rb	ND	92 (11)
Sr	ND	ND
Y	6333 (452)	5885 (54)
Zr	496162 (1606)	1846 (38)
Nb	ND	20607 (111)
Mo	ND	149 (20)
Pb	ND	247 (30)
Th	ND	10183 (104)
U	1180	211 (27)

Major-element oxides by electron microprobe. Total Fe expressed as FeOT. Trace elements by PIXE except Fe (by EMP). – = not analyzed. ND = not detected by PIXE analysis. 1 sigma errors in parentheses.

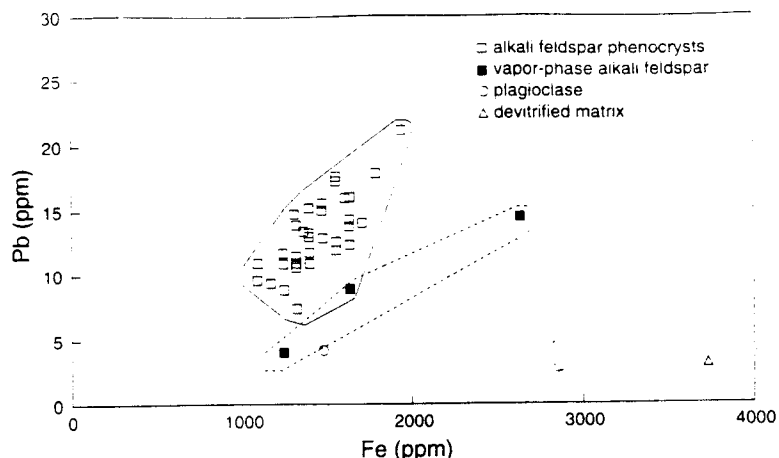


Fig. 9. Pb (ppm) versus Fe (ppm) for feldspar phenocrysts and vapor-phase overgrowths determined by PIXE. Concentrations of Fe (1200–1600 ppm), Zn (3–9 ppm), Ga (23–40 ppm), Rb (10–120 ppm), Sr (< 10–100 ppm), Ba (400–1600 ppm), and Pb (7–16 ppm) in alkali-feldspar phenocrysts are moderately well correlated with feldspar composition and stratigraphic position. Concentrations of Fe, Zn, Ga, Rb and Pb increase with increasing mol.% Or, whereas Sr and Ba decrease with increasing mol.% Or. However, Pb has perhaps the poorest correlation of these elements.

high concentrations of Cd, Pb, Cu and Zn obtained in acid-leaching experiments of fresh ash (Smith et al., 1982). It is not known to what extent > 1 million years of post-emplacement hydrothermal and low-temperature diagenetic alteration has affected trace-metal concentrations in the UBT. Keith (1991) has observed that much of the chloride and sulfate-rich encrustations described by early expeditions to the VTTS (1917–1919) were removed by the time of her study.

Data for concentrations of metals in thermal waters draining from recently emplaced ash-flow tuffs are scarce, with perhaps the most data available from the Pumice Plain at Mount St. Helens. Comparison of data collected in June, 1980 by Dethier et al. (1981) with data collected from 1985 to 1989 by Shevenell and Goff (1993) indicate an approximately ten-fold decline in Co, Cu and Pb concentrations in thermal waters issuing from the deposits shortly after the time of eruption to summer of 1985. By 1985 Pb was largely below detection (< 0.002 mg/l) in thermal waters; however, Cu and Zn remained above detection in two hot springs repeatedly sampled by Shevenell and Goff (1993). Cu showed declining concentration with time in these springs, whereas Zn showed no clear trend with time. These data suggest that some fraction of metals such as Co, Cu and Pb

are easily leachable from non-welded ash for a short period after deposition (Shevenell, pers. commun., 1995).

5.3. Comparison of the UBT vapor-phase mineral suite to volcanic sublimates

Magmatic volatiles are strongly enriched in alkaline and rare metals relative to their parent silicate melts, with chalcophile metals (Cd, Cu, In, Pb and Tl) being especially abundant in vapor (Zoller et al., 1983; Symonds et al., 1987; Bernard et al., 1990; Kyle et al., 1990). Pb in particular is commonly enriched in volcanic gases relative to source magma by three to five orders of magnitude, and surpasses the concentration of common rock-forming elements in some systems (Kavalieris, 1994; Hinkley et al., 1994). Similarly, data from fossil fumaroles and active fumarolic assemblages indicate that sublimates are strongly enriched in metal-bearing minerals deposited from these vapors (Keith, 1991; Symonds, 1993).

Fumarolic sublimates are commonly zoned (Stoiber and Rose, 1974), and this zonal pattern of mineral precipitation has been reproduced in silica tubes inserted into fumaroles (Le Guern and Bernard, 1982). In most cases the highest temperature and

most reduced assemblages are nearest the vent. At Mount St. Helens and Merapi volcanoes, cristobalite and magnetite are typical of the highest temperature zones (> 800 to 650°C), and are commonly accompanied by sulfides of Pb and Bi (Symonds et al., 1987; Symonds and Reed, 1993). At Mount St. Helens, intermediate-temperature assemblages (black crusts formed at 550–450°C) contain these same minerals plus Pb oxide, whereas lower-temperature assemblages lack Pb minerals (Symonds and Reed, 1993). At Merapi, however, lower-temperature assemblages contain various alkali and metal sulfates and chlorides, including Pb-bearing species (Symonds et al., 1987; Kavalieris, 1994).

In the Bandelier system, trace-mineral assemblages in glassy samples are dominated by metal oxides, sulfides and carbonates. We suggest that at least some of these minerals were precipitated directly from magmatic vapors. In devitrified samples, vapor-phase alkali feldspar, cristobalite and magnetite certainly began growing at the highest temperatures, analogous to temperatures measured for fumarolic sublimates. These temperatures may have ranged as high as 600 to 740°C assuming eruption temperatures of ~ 700–840°C (Warsaw and Smith, 1988) and ~ 100°C of eruptive cooling (fumarole temperatures as high as 645°C were recorded in 1919 in a similar setting at the VTTS). The abundance of alkali feldspar in the vapor-phase assemblage of silicic tuffs as compared to sublimates presumably reflects the higher alkali content and higher rock:gas ratio of cooling ash sheets relative to the fumarolic vents developed on the dacitic-to-basaltic andesite volcanoes cited above. These factors are also apparently responsible for the relative abundance of phases rich in incompatible elements (P, Zr, Nb, Y, LREE), which are concentrated by at least an order of magnitude in high-silica rhyolites relative to dacitic rocks. Some of these incompatible element-rich minerals were crystallizing from the most evolved magma in the Bandelier chamber at the time of eruption (zircon, monazite, apatite), and thus it is likely that they were also stable in the highest temperature vapors. Other minerals such as titanite and unidentified oxides (?) of Ba, Y, Nb and LREE may have grown at lower temperatures, under more oxidizing conditions.

The abundance of Pb and Bi sulfides in high-temperature sublimate assemblages suggests that these

minerals may have begun forming directly from magmatic vapor and continued to form during the earliest stages of cooling in the Bandelier Tuff. Conversely, sulfates, carbonates and phosphates are more typical of lower-temperature sublimate assemblages and probably began crystallizing at later times. It is more difficult to determine the timing of crystallization of chlorides and oxides in the Bandelier assemblage, but these minerals commonly form at intermediate temperatures in sublimate assemblages, with chlorides becoming increasingly important in lower-temperature assemblages. The general lack of water-soluble chlorides and sulfates in the Bandelier ignimbrite is probably due to its long exposure time relative to pristine sublimate assemblages. The accumulation of halite and gypsum where fractures pass downward into relatively unfractured, non-welded tuffs suggests that these minerals were leached from the overlying section and evaporatively concentrated, although trace amounts of these minerals are also found associated with near-surface clays that are soil-derived (Vaniman and Chipera, unpubl. Los Alamos National Lab report).

The alteration assemblage developed on pyroxene and fayalite phenocrysts in devitrified samples appears to have formed during crystallization and cooling of the unit because the assemblage is virtually absent in glassy samples. The presence of smectite implies temperatures of < 150°C, but we believe that alteration began at much higher temperatures because, in addition to smectite and hematite, the assemblage includes trace-metal-rich minerals typical of high-temperature sublimates. In a detailed examination of a nearly identical assemblage from the VTTS, Spilde et al. (1993) also concluded that alteration of pyroxene by acidic vapors began at temperatures as high as 400°C. We speculate that the mafic silicates in the UBT were originally altered to illite, or some other clay, which transformed to smectite at temperatures of 100 to 300°C (e.g., Velde and Meunier, 1987).

6. Conclusions

A wide variety of trace metals (e.g., Pb, Bi, Sb, As, Cu, Ag, Re) are partitioned into the vapor-phase during eruption and devitrification of silicic tuffs and

flows, and thus their whole-rock abundances may be modified from their distribution in the source magma. These metals are deposited as micron-scale mineral coatings in porous tuff, and thereby are available for further redistribution by groundwater or hydrothermal fluids. In the Bandelier Tuff, a suite of metal-bearing trace phases similar to those found in volcanic fumaroles formed in trace quantities throughout the unit, and more abundantly in zones of focused vapor transport. Combined mineralogic and whole-rock geochemical data confirm that aside from areas of extensive vapor transport, elements such as Pb were only locally remobilized during devitrification and vapor-phase crystallization. In devitrified portions of the unit, a high proportion of the Pb, and associated metals such as Sb, Cu, Ag and Re reside in Pb minerals or associated with smectite and hematite alteration of mafic silicate phenocrysts. These metals may be readily scavenged by hydrothermal fluids to form mineral deposits in some long-lived volcanic centers.

Acknowledgements

Caleb Evans, Carl Maggiore, and Mark Hollander of the Los Alamos Ion-beam Lab facilitated the PIXE work. Thanks to Dale Counce who assisted with GFAA analyses, Peggy Snow who assisted with EMP analyses, Dave Mann who prepared polished sections, and Barry Moore and James Archuleta who drafted figures. Journal reviews by N. Dunbar and T.A. Vogel, and informal reviews by D. Vaniman and F. Goff improved the clarity and content of the original manuscript. This research was supported by a Los Alamos Directed Research and Development Grant to D. Hickmott. J. Wolff received support from Associated Western Universities.

References

- Anderson Jr., A.T., 1991. Hourglass inclusions: theory and application to the Bishop rhyolite tuff. *Am. Mineral.*, 76: 530–554.
- Bailey, R.A., Smith, R.L. and Ross, C.S., 1969. Stratigraphic nomenclature of the volcanic rocks in the Jemez Mountains, New Mexico. *U.S. Geol. Surv., Bull.* 1274-P, 19 pp.
- Balsley, S.D., 1988. The petrology and geochemistry of the Tshirege member of the Bandelier Tuff, Jemez Mountains Volcanic Field, New Mexico, USA. M.S. Thesis, U.T. Austin, 188 pp.
- Bernard, A., Symonds, R.B. and Rose Jr., W.I., 1990. Volatile transport and deposition of Mo, W and Re in high temperature magmatic fluids. *Appl. Geochem.*, 5: 317–326.
- Bish, D.L. and Chipera, S.J., 1988. Problems and solutions in quantitative analysis of complex mixtures by X-ray powder diffraction. *Adv. X-Ray Anal.*, 31: 295–308.
- Blake, S. and Ivey, G.N., 1986. Density and viscosity gradients in zoned magma chambers, and their influence on withdrawal mechanics. *J. Volcanol. Geotherm. Res.*, 30: 201–230.
- Bodnar, R.J., Mavrogenes, J.A., Anderson, A.J., Baft, S., Rivers, M.L. and Sutton, S.R., 1993. Synchrotron XRF analyses of synthetic fluid inclusions. *Eos*, 74(43): 669.
- Broxton, D.E. and Reneau, S.L., 1995. Stratigraphic nomenclature of the Bandelier Tuff for the Environmental Restoration Project at Los Alamos National Laboratory. LA-13010-MS, 21 pp.
- Broxton, D.E., Heiken, G., Chipera, S.J. and Byers Jr., F.M., 1995. Stratigraphy, petrography, and mineralogy of tuffs at Technical area 21. Los Alamos Natl. Lab., New Mexico. LA-12934-MS, 31 pp.
- Burnett, D.S., Woolum, D.S., Benjamin, T.M., Rogers, P.S.Z., Duffy, C.J. and Maggiore, C., 1988. High precision thick target PIXE analyses of Carbonaceous meteorites. *Nucl. Instrum. Methods Phys. Res.*, B35: 67–74.
- Burt, D.M. and Sheridan, M.F., 1981. A model for the formation of uranium/lithophile element deposits in fluorine-enriched volcanic rocks. *Am. Assoc. Pet. Geol. Stud. Geol.*, 13: 99–109.
- Caress, M., 1994. Feldspar compositions from the Bandelier Tuff, New Mexico: insights into magma chamber processes. *Geology*, 75(44): 748–749.
- Christiansen, E.H., Sheridan, M.F. and Burt, D.M., 1986. The geology and geochemistry of Cenozoic topaz rhyolites from the western United States. *Geol. Soc. Am., Spec. Pap.* 205, 82 pp.
- Chung, F.H., 1974. Quantitative interpretation of X-ray diffraction patterns of mixtures. I. Matrix-flushing method for quantitative multicomponent analysis. *J. Appl. Crystallogr.*, 7: 519–525.
- Crowe, G.M., Linn, G.W., Heiken, G. and Bevier, M.L., 1978. Stratigraphy of the Bandelier Tuff in the Pajarito Plateau. *Applications to Waste Management*. LA-7225-MS, 57 pp.
- Czamanske, G.K., Sission, T.W., Campbell, J.L. and Teesdale, W.J., 1993. Micro-PIXE analysis of silicate reference standards. *Am. Mineral.*, 78: 893–903.
- Dethier, D.P., Frank, D. and Pevear, D.R., 1981. Chemistry of thermal waters and mineralogy of the new deposits at Mount St. Helens—A preliminary report. *U.S. Geol. Surv., Prof. Pap.* 81-80, 24 pp.
- Duffy, C.J., Rogers, P.S.Z. and Benjamin, T.M., 1987. The Los Alamos PIXE data reduction software. *Nucl. Instrum. Methods Phys. Res.*, B22: 91–95.
- Dunbar, N.W. and Hervig, R.L., 1992. Volatile and trace element composition of melt inclusions from the Lower Bandelier

- Tuff: implications for magma chamber processes and eruptive style. *J. Geophys. Res.*, 97: 15,151–15,170.
- Farrah, H. and Pickering, W.C., 1977. The sorption of lead and cadmium species by clay minerals. *Aust. J. Chem.*, 30: 1417–1422.
- Fisher, R.V., 1979. Models for pyroclastic surges and pyroclastic flows. *J. Volcanol. Geotherm. Res.*, 6: 305–318.
- Goff, F., Stimac, J.A., Larocque, A.C.L., Hulen, J.B., McMurtry, G.M., Adams, A.I., Roldan, M.A., Trujillo Jr., P.E., Counce, D., Chipera, S.J., Mann, D. and Heizler, M., 1994. Gold degassing and deposition at Galeras Volcano, Colombia. *GSA Today*, 4(10): 241–247.
- Hildreth, W., 1979. The Bishop Tuff: Evidence for the origin of compositional zoning in magma chambers. *Geol. Soc. Am. Spec. Pap.*, 180: 43–75.
- Hildreth, W., 1981. Gradients in silicic magma chambers: implications for lithospheric magmatism. *J. Geophys. Res.*, 86: 10,153–10,192.
- Hinkley, T.K., Le Cloarec, M.-F. and Lamber, G., 1994. Fractionation of families of major, minor, and trace metals across the melt–vapor interface in volcanic exhalations. *Geochim. Cosmochim. Acta*, 58: 3255–3263.
- Izett, G.A. and Obradovich, J.D., 1994. $^{40}\text{Ar}/^{39}\text{Ar}$ age constraints for the Jaramillo Normal Subchron and the Matuyama–Brunhes geomagnetic boundary. *J. Geophys. Res.*, 99: 2925–2934.
- Malavaleris, I., 1994. High Au, Ag, Mo, Pb, V and W content of a fumarole deposit at Merapi volcano, central Java, Indonesia. *J. Geochem. Explor.*, 50: 479–491.
- Keith, T.E.C., 1991. Fossil and active fumaroles in the 1912 eruptive deposits, Valley of Ten Thousand Smokes, Alaska. *J. Volcanol. Geotherm. Res.*, 45: 227–254.
- Kuentz, D.A., 1986. The Otowi member of the Bandelier Tuff: A study of the petrology, petrography, and geochemistry of an explosive silicic eruption, Jemez Mountains, New Mexico. M.S. Thesis, Univ. Texas, Arlington, TX, 168 pp.
- Kyle, P.R., Meeker, K. and Finnegan, D., 1990. Emission rates of sulfur dioxide, trace gases and metals from Mt. Erebus, Antarctica. *Geophys. Res. Lett.*, 50: 2125–2128.
- Le Guern, F. and Bernard, A., 1982. A new method for sampling and analyzing volcanic sublimes—application to Merapi volcano, Java. *J. Volcanol. Geotherm. Res.*, 12: 133–146.
- Lipman, P.W., Christiansen, R.L. and O'Connor, J.T., 1966. A compositionally zoned ash-flow sheet in southern Nevada. *U.S. Geol. Surv. Prof. Pap.* 524-F, 47 pp.
- Lowenstern, J.B., 1993. Evidence for a copper-bearing fluid in magma erupted at the Valley of Ten Thousand Smokes, Alaska. *Contrib. Mineral. Petrol.*, 114: 409–421.
- Lowenstern, J.B., 1994. Chlorine, fluid immiscibility, and degassing in peralkaline magmas from Pantelleria, Italy. *Am. Mineral.*, 79: 353–369.
- Lowenstern, J.B., Mahood, G.A., River, M.L. and Sutton, S.R., 1991. Evidence for extreme partitioning of copper into a magmatic vapor phase. *Science*, 252: 1405–1409.
- Macdonald, R., Smith, R.L. and Thomas, J.E., 1992. Chemistry of subalkalic silicic obsidians. *U.S. Geol. Surv. Prof. Pap.* 1523, 214 pp.
- Meeker, K.A., Chuan, R.L., Kyle, P.R. and Palais, J.M., 1991. Emission of elemental gold particles from Mount Erebus, Ross Island, Antarctica. *Geophys. Res. Lett.*, 18(8): 1405–1408.
- NOT IN REFERENCE LIST: PLEASE SUPPLY
- Papike, J.J., Keith, T.E.C., Spilde, M.N., Galbreath, K.C., Shearer, C.K. and Laul, J.C., 1991. Geochemistry and mineralogy of fumarolic deposits, Valley of Ten Thousand Smokes, Alaska: bulk chemical and mineralogical evolution of dacite-rich protoliths. *Am. Mineral.*, 76: 1661–1673.
- Pouchou, J.L. and Pichoir, F., 1985. "PAP" Phi(Rho-Z) procedure for improved quantitative microanalysis. In: J.T. Armstrong (Editor), *Microbeam Analysis*. San Francisco Press, San Francisco, CA, pp. 104–105.
- Ross, C.S. and Smith, R.L., 1961. Ash-flow tuffs: their origin, geologic relations, and identification. *U.S. Geol. Surv. Prof. Pap.* 366, 55 pp.
- Self, S., Goff, F., Gardner, J.N., Wright, J.V. and Kite, W.M., 1986. Explosive rhyolitic volcanism in the Jemez Mountains: vent locations, caldera development and relation to regional structure. *J. Geophys. Res.*, 91: 1779–1798.
- Shevenell, L. and Goff, F., 1993. Addition of magmatic volatiles into the hot spring waters of Loowit Canyon, Mount St. Helens, Washington, USA. *Bull. Volcanol.*, 55: 489–503.
- Smith, D.B., Zielinski, R.A. and Rose Jr., W.I., 1982. Leachability of uranium and other elements from freshly erupted volcanic ash. *J. Volcanol. Geotherm. Res.*, 13: 1–30.
- Smith, R.L., 1960. Zones and zonal variations in welded ash flows. *U.S. Geol. Surv. Prof. Pap.* 354-F, 55 pp.
- Smith, R.L., 1979. Ash-flow magmatism. *Geol. Soc. Am. Spec. Pap.*, 180: 5–28.
- Smith, R.L. and Bailey, R.A., 1966. The Bandelier Tuff: a study of ash-flow eruption cycles and zoned magma chambers. *Bull. Volcanol.*, 29: 83–104.
- Soldatini, G.F., Riffaldi, R. and Minzi, R.L., 1976. Pb sorption by soils. *Water, Air Soil Pollut.*, 22: 111–118.
- Spilde, M.N., Brearley, A.J. and Papike, J.J., 1993. Alteration of plagioclase and pyroxene phenocrysts in a fissure fumarole, Valley of Ten Thousand Smokes, Alaska. *Am. Mineral.*, 78: 1066–1081.
- Stimac, J.A., in press. Hornblende dacite pumice in the Tshirege Member of the Bandelier Tuff: implications for magma chamber and eruptive processes. *N. M. Geol. Soc. Guideb.*, 47th Field Conf., Sept. 25–28 (Jemez Mountains Region).
- Stimac, J. and Hickmott, D., 1994. Trace-element partition coefficients for ilmenite, orthopyroxene, and pyrrhotite in rhyolite determined by micro-PIXE analysis. *Chem. Geol.*, 117: 313–330.
- Stimac, J.A., Clark, A.H., Chen, Y. and Garcia, S., 1995. Enclaves and their bearing on the origin of the Cornubian batholith. *Mineral. Mag.*, 59: 273–296.
- Stix, J., Goff, F., Gorton, M.P., Heiken, G. and Garcia, S., 1988. Restoration of compositional zonation in the Bandelier silicic magma chamber between two caldera-forming eruptions: geochemistry and origin of the Cerro Toledo Rhyolite, Jemez Mountains, New Mexico. *J. Geophys. Res.*, 93: 6129–6147.
- Stoiber, R.E. and Rose Jr., W.I., 1974. Fumarole incrustations at active Central American volcanoes. *Geochim. Cosmochim. Acta*, 38: 495–516.

- Symonds, R., 1993. Scanning electron microscope observations of sublimates from Merapi Volcano, Indonesia. *Geochem. J.*, 26: 337–350.
- Symonds, R.B. and Reed, M.H., 1993. Calculation of multicomponent chemical equilibria in gas–solid–liquid systems: calculation methods, thermochemical data, and application to studies of high-temperature volcanic gases with examples from Mount St. Helens. *Am. J. Sci.*, 293: 758–864.
- Symonds, R., Rose Jr., W.I., Reed, M.H., Lichte, F.E. and Finnegan, D.L., 1987. Volatilization, transport and sublimation of metallic and non-metallic elements in high temperature gases at Merapi Volcano, Indonesia. *Geochim. Cosmochim. Acta*, 51: 2083–2101.
- Vaniman, E. and Wohletz, K., 1990. Results of geologic mapping/fracture studies: TA-55 area. Los Alamos Natl. Lab. Seismic Hazards Memo EES-1-SH90-17, 25 pp.
- Velde, D. and Meunier, A., 1987. Petrologic phase equilibria in natural clay systems. In: A.C.D. Newman (Editor), *Chemistry of Clays and Clay Minerals*. Mineral. Soc. Monogr., 6: 423–458.
- Wallace, P.J. and Gerlach, T.M., 1994. Magmatic vapor source for sulfur dioxide released during volcanic eruptions: evidence from Mount Pinatubo. *Science*, 265: 497–499.
- Warshaw, C.M. and Smith, R.L., 1988. Pyroxenes and fayalite in the Bandelier Tuff, New Mexico: temperatures and comparison with other rhyolites. *Am. Mineral.*, 73: 1025–1037.
- Webster, J.D. and Duffield, W.A., 1991. Volatiles and lithophile elements in Taylor Creek Rhyolite: constraints from glass inclusion analysis. *Am. Mineral.*, 76: 1628–1645.
- Webster, J.D. and Duffield, W.A., 1994. Extreme halogen abundances in Tin-rich magma of the Taylor Creek Rhyolite, New Mexico. *Econ. Geol.*, 89: 840–850.
- Zielinski, R.A., Lipman, P.W. and Millard Jr., H.T., 1977. Minor-element abundances in obsidian, perlite, and felsite of calc-alkalic rhyolites. *Am. Mineral.*, 62: 426–437.
- Zoller, W.H., Parrington, J.R. and Kotra, J.M.P., 1983. Iridium enrichment in airborne particles from Kilauea volcano. *Science*, 222: 1118–1120.